END-2011-0671-ver9-Zhou_1P
Type: research-article

JOURNAL OF ENDOUROLOGY
Volume 26, Number 00, XXXX 2012

Pp. ■■■–■■■
DOI: 10.1089/end.2011.0671

Reduction of Bubble Cavitation by Modifying the Diffraction Wave from a Lithotripter Aperture

Yufeng Zhou, Ph.D.

Abstract

Purpose: A new method was devised to suppress the bubble cavitation in the lithotripter focal zone to reduce the propensity of shockwave-induced renal injury.
Materials and Methods: An edge extender was designed and fabricated to fit on the outside of the ellipsoidal reflector of an electrohydraulic lithotripter to disturb the generation of diffraction wave at the aperture, but with little effect on the acoustic field inside the reflector.
Results: Although the peak negative pressures at the lithotripter focus using the edge extender at 20 kV were similar to that of the original configuration (-11.1 ± 0.9 *vs* −10.6 ± 0.7 MPa), the duration of the tensile wave was shortened significantly (3.2 ± 0.54 *vs* 5.83 ± 0.56 μs, $P < 0.01$). There is no difference, however, in both the amplitude and duration of the compressive shockwaves between these two configurations as well as the −6 dB beam width in the focal plane. The significant suppression effect of bubble cavitation was confirmed by the measured bubble collapse time using passive cavitation detection. At the lithotripter focus, while only about 30 shocks were needed to rupture a blood vessel phantom using the original HM-3 reflector at 20 kV, no damage could be produced after 300 shocks using the edge extender. Meanwhile, the original HM-3 lithotripter at 20 kV can achieve a stone comminution efficiency of 50.4 ± 2.0% on plaster-of-Paris stone phantom after 200 shocks, which is comparable to that of using the edge extender (46.8 ± 4.1%, $P = 0.005$).
Conclusions: Modifying the diffraction wave at the lithotripter aperture can suppress the shockwave-induced bubble cavitation with significant reduced damage potential on the vessel phantom but satisfactory stone comminution ability.

Introduction

Since its introduction in the early 1980s, shockwave lithotripsy (SWL) has revolutionized the treatment for patients with upper urinary stone disease.[1] Despite its great success and the development of several generations of clinical lithotripters with friendly user interface, better imaging quality, less anesthesia requirement, multifunctionality, and sometimes, high cost-effectiveness for stone treatment in the past three decades, no fundamental improvement in SWL technology has been accomplished.[2] In particular, there is substantial evidence from both clinical and basic studies that SWL produces acute renal injury, such as hematuria, kidney enlargement, renal and perirenal hemorrhage, and hematomas.[3–6]

SWL-induced vascular injury along the shockwave propagation path throughout the thickness of the kidney[7] is characterized by extensive damage of the endothelial cells and rupture of the blood vessels, with capillary and small blood vessels much more susceptible to SWL injury than the large ones.[3–4] Although most patients recover well after lithotripsy, there are subgroups of patients who are at much higher risk for chronic injury.[4] These include patients with solitary kidneys, preexisting hypertension, and, in particular, elderly patients.[7] Therefore, reduction of SWL-induced renal injury is of importance for both clinician and stone patients.

Two competing mechanisms have been implicated for SWL-induced tissue injury: Cavitation and shear stress. Shear deformation from a shock front propagating through a heterogeneous medium[8] could be accumulated if the relaxation time of a tissue (ie, with a large interstitial volume) is comparable to clinical shock delivery rate (~ 1 Hz), which predicts that hemorrhage would first appear in the inner medulla and broader focal zone at the same peak pressure would cause less renal damage.[9]

Previous studies have shown that bubble cavitation could damage nearby objects via either the high pressure and temperature produced during symmetric collapse or high-speed microjet formed during asymmetric collapse.[10–12] Animal studies using a pressure-release reflector, which reduces bubble cavitation and maintains the effect of shear stress simultaneously, demonstrated minimal tissue damage at a

Division of Engineering Mechanics, School of Mechanical & Aerospace Engineering, Nanyang Technological University, Singapore.

clinical dose of 2000 shocks at 16 ~ 24 kV, which favor cavitation over shear stress as the primary mechanism for tissue injury.[13]

Using vessel phantoms made of single cellulose hollow fibers, bubble dynamics inside a constrained medium has been investigated.[14] It was found that the rapid intraluminal bubble expansion leads to a significant dilation of the vessel wall and a rupture if the resultant circumferential hoop stress exceeds the failure strength of the vessel. Furthermore, a high-speed micrograph of the bubble dynamics inside an *ex vivo* artery of rat mesenteries (smaller than 20 μm) under a two-cycle high-intensity focused ultrasound burst shows that liquid jets (directed away from the nearest vessel wall), vessel distention (motion outward against the surrounding tissue), and vessel invagination (motion inward toward the lumen) can contribute to vessel rupture. In that situation, invagination is found to exceed distention as indicated by bubble fragments growing outside the vessel and dye extravasation.[15]

To reduce SWL-induced vascular injury, several approaches have been proposed. Although the use of a pressure release reflector can suppress maximum bubble expansion and result in a significant reduction of vascular injury *in vivo*, the inversion of a lithotripsy shockwave (LSW) also diminishes the stone fragmentation.[13,16,17] A small overpressure (~4 bars) applied to the lithotripter field could increase the cavitation threshold and subsequently suppress the bubble activities.[18] *In-situ* pulse superposition technique is using an ellipsoidal reflector insert to separate the focusing LSW into two parts and then to superpose the almost compressive pulse from the remaining original reflector on the tensile component of LSW from the reflector insert.[19,20] *In vitro* experiments have shown the reduction on bubble cavitation without compromising the stone comminution ability. Acoustic diode (AD), consisting of two membranes in a vacuum chamber, allows the passage of compressive wave, but not the tensile wave from the mechanical response of these membranes and the resultant acoustic impedance of AD.[21]

Although suppression of bubble cavitation can be achieved successfully, the installation or removal of those devices in the lithotripter is not convenient during a clinical SWL treatment. Therefore, a simple and reliable protection apparatus for SWL treatment is in great need.

In this study, a novel method was developed to modify the LSW waveform to suppress the bubble cavitation in SWL. An edge extender with acoustic absorbing material was fitted at the aperture of a clinical Dornier HM-3 lithotripter to modify the generation of diffraction wave. Experiments were performed to characterize the physical properties of the modified lithotripter field (pressure waveform, acoustic emission, and bubble dynamics) and to assess the lithotripter performance (stone comminution and vessel phantom rupture). It was found that the edge extender could significantly and consistently suppress bubble cavitation in the lithotripter focal zone, resulting in the reduced potential for vessel phantom damage but satisfactory stone fragmentation ability.

Materials and Methods

Shockwave evolution

Linear propagation (ie, wave reflection, focusing, and diffraction) of a shockwave along the lithotripter axis is described as:[22]

$$\frac{p_2}{p_0} = H_c(z)f(\tau_c) + H_e(z)f(\tau_e) + \frac{C_0}{a}\int_{t_1}^{t_2} H_w(z,t')f(t-t')dt' \quad (1)$$

The contribution of center wave (c), edge wave (e), or the diffraction wave at the reflector aperture and wake (w) to LSW were illustrated as the three items on the right side of Eq. 1, respectively. These three waveform components are also clear in the simulated waveforms using a nonlinear Khokhlov-Zabolotskaya-Kuznetsov (KZK) equation (Fig. 1).[23,24] Although the spark discharge between electrode tips produces an almost compressive wave, the tensile component of LSW (consisting of the wake and the edge wave in the prefocal region) appears slightly above the reflector aperture (Fig. 1a). As the shockwave propagates toward the focal point, the edge wave moves toward the center wave and merges with the wake (Fig. 1c). The acoustic energy stored in the tensile part of LSW is the primary mechanism for bubble cavitation.[14,25] Therefore, if a soft boundary, similar to the passive noise barrier, presents on the reflector aperture,[26,27] the production of edge wave will be modified for fewer contributions to the tensile wave. Consequently, the bubble expansion energy will become smaller, and the propensity of SWL-induced tissue injury will be reduced. ◀F1

The distribution of the acoustic ray inside the ellipsoidal reflector is nonuniform with more energy concentrating in the center than at the edge.[20,22] Therefore, there will be a negligible change on the center wave of LSW, if only the edge condition is modified. As a result, the effectiveness of the stress wave, which dominates the initial stone comminution,[28] will be maintained.

Lithotripter and edge extender

The experiment was carried out in a Dornier HM-3 lithotripter with an 80 nF capacitor and a truncated brass ellipsoidal reflector (Fig. 2b). A prototype edge extender was fabricated and fitted at the aperture of the HM-3 lithotripter, which consists of eight trapezoidal segments (size of 72–100 × 70 mm and the angle with respect to the lithotripter axis of ~31.5 degrees) (Fig. 2c). Each segment, essentially comprising acoustic absorbent material (a piece of wavy foam) attached to a supporting Lucite plate, was connected with an adaptor ring via a hinge (Fig. 2a). To ensure smooth transition of boundary condition, the edge extender covers the inner surface of the ellipsoidal reflector by about 5 mm. If the edge extender is not in use, each segment can be rotated outward to diminish the influence on the lithotripter field. ◀F2

Pressure field mapping

The LSW profile was measured using a light spot hydrophone (LSHD, Siemens, Germany).[29,30] A laser light source at the rear side of a quartz block (in air) was focused into a small spot (50 μm) on the front side, which was immersed in water perpendicular to the propagation path of LSWs, and the reflected laser light was picked up by a broad bandwidth photo detector. Pressure waveform can then be calculated using a program provided by the manufacturer.[31] The LSHD was attached to a three-dimensional position system (Velmex, Bloomfield, NY) with a minimum step size of 5 μm and titled at a 14-degree angle from the horizontal plane to align normal to the axis of the HM-3 lithotripter (Fig. 3). A mechanical ◀F3

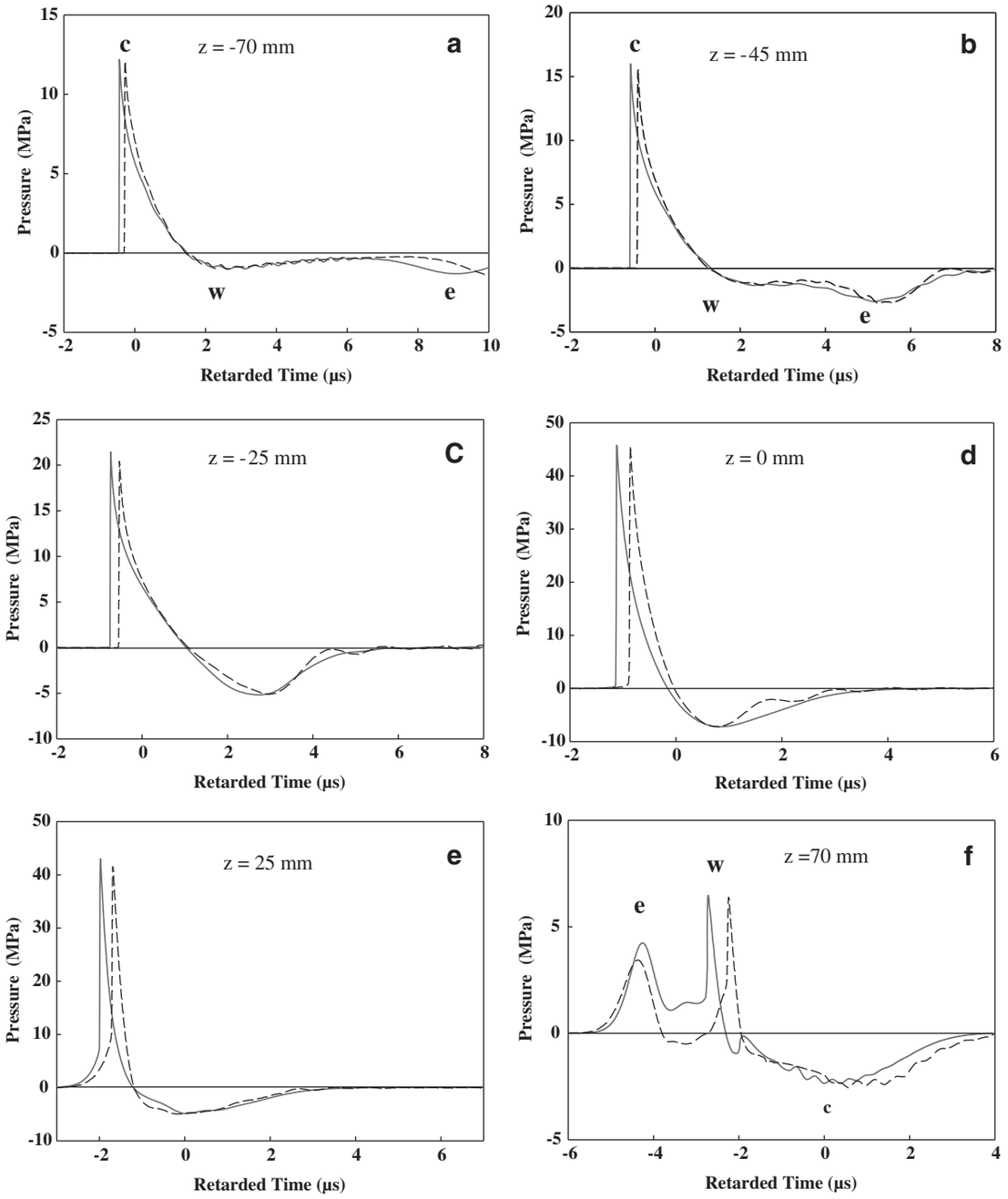

FIG. 1. Theoretical prediction of pressure waveforms along the HM-3 lithotripter axis by Khokhlov-Zabolotskaya-Kuznetsov equation using the original HM-3 reflector at (a) z = −70 mm, (b) z = −45 mm, (c) z = 25 mm, (d) z = 0 mm, (e) z = 25 mm, and (f) z = 70 mm using the original reflector (solid line) and the edge extender (dash line). C = center wave, w = wake, e = edge wave.

pointer was used to align the laser spot with the focal point of the lithotripter.[20] A LabVIEW (National Instruments, Austin, TX) program controlled the automatic field mapping in a step size of 1 mm. At each location, at least six samples were recorded by a digital oscilloscope (LeCroy 9304, Chestnut Ridge, NY) operated at 100 MHz sampling rate, and the data were subsequently transferred to a PC for off-line analysis.

Passive cavitation detection

A 1 MHz focused transducer (V392-SU, Olympus-IMS, Waltham, MA) with a focal length of 100 mm and a −6 dB beam diameter of 4 mm was used to measure the acoustic emission (AE) associated with bubble oscillations in water (Fig. 3).[14,19] The focused transducer, attached to a three-axis

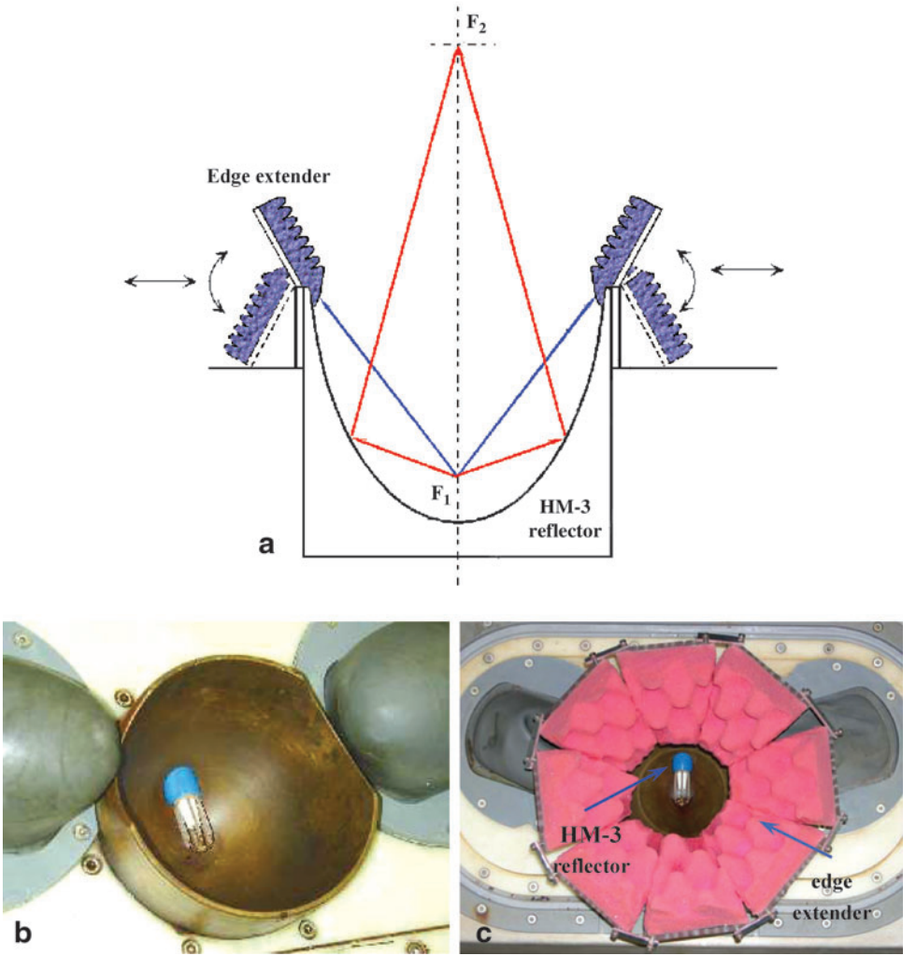

4C ▶

FIG. 2. **(a)** The schematic diagram of the edge extender fitted with the original HM-3 reflector. Photographs show **(b)** the original reflector and **(c)** the edge extender in the Dornier HM-3 lithotripter. The edge extender has eight segments with each one being able to operate individually.

translational stage, was first aligned confocally with the lithotripter focus, and then scanned along and transverse to the lithotripter axis in a step size of 5 mm and 2.5 mm, respectively. Ten AE signals were recorded at each position.

Stone comminution

The stone comminution ability of the lithotripter was tested using established protocols (Fig. 3).[19,20] A chamber with a slab of tissue mimicking phantom (25.4 × 2.54 cm, D × H) and an acoustic transparent polyester membrane at the bottom was filled with fresh castor oil and then positioned with the lithotripter focus on its central axis. The spherical stone phantom (D = 10 mm) made of plaster-of-Paris with a powder to water ratio of 1.5:1 by weight was immersed in degassed water for at least 2 hours until no visible bubble could be observed, and then placed into a plastic cylindrical holder that was connected to the hydraulic gantry of the HM-3 system so that the stone phantom could be aligned to lithotripter focus under the guidance of a biplanar fluoroscopic imaging. A total of 200 shocks were delivered to the stone phantoms at a pulse repetition rate of 1 Hz at the output voltage of 20 kV. After the exposure, all fragments were carefully removed from the holder, spread out into a layer on paper, and let dry at room temperature for 24 hours. The dry fragments were then filtered through a series of American Society for Testing and Materials standard sieves (W.S. Tyler, Mentor, Ohio) with 4, 2.8, and 2 mm grids. Stone comminution efficiency was determined by the percentage of fragments less than 2 mm. Six samples were used under each test configuration.

Vessel phantom rupture

The propensity of vascular injury produced by the LSWs was evaluated using a vessel phantom made of a single cellulose hollow fiber (132290, Spectrum, Gardena, CA) with 200 μm inner diameter and 8 μm wall thickness.[14] Degassed water (O_2 concentration < 4 mg/L), seeded with 0.1% contrast agent Optison (Amershan Health, Princeton, NJ) by volume, was circulated by a peristaltic pump (7619-50, Cole-Parmer, Vernon Hills, IL). The vessel phantom was immersed in the testing chamber with fresh castor oil to minimize cavitation activities outside it. A low pulse repetition rate (< 0.1 Hz) was used so that before each shockwave exposure, any visible

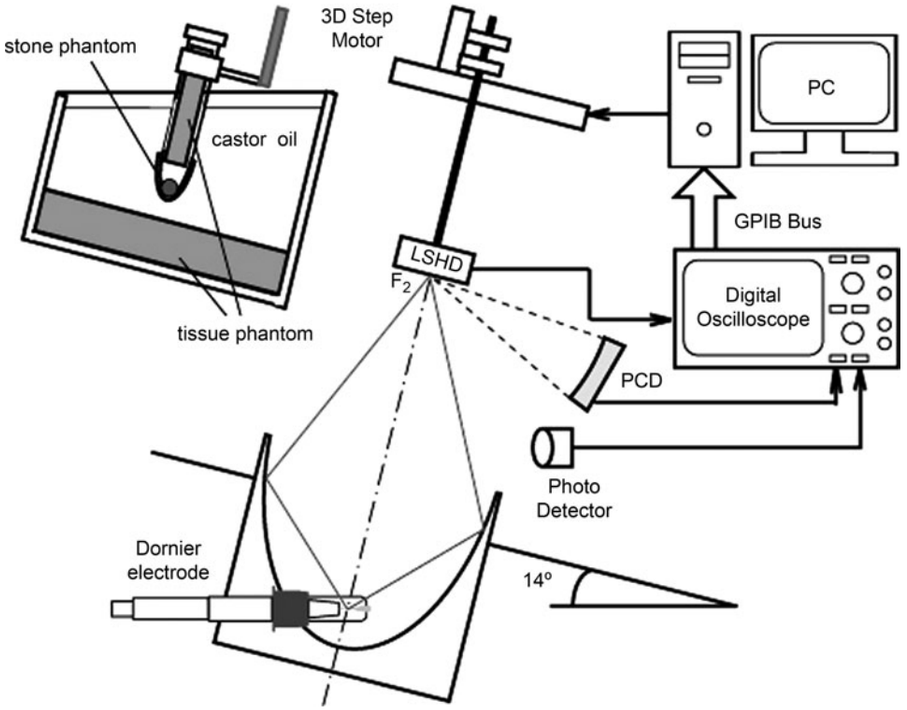

FIG. 3. The experimental setup for pressure mapping by a light spot hydrophone, passive cavitation measurement, and stone comminution in a Dornier HM-3 lithotripter. Tissue mimicking phantoms were used to simulate the effects of tissue attenuation on incident lithotripter shockwaves.

bubbles outside the vessel phantom can be removed carefully. Rupture of the vessel phantom can be easily identified because the circulating fluid will leak out and form a droplet in the castor oil at the rupture site. At this moment, the experiment was stopped, and the number of shockwaves delivered was recorded. If there was no rupture after 300 shocks, the experiment would also be terminated. A total of six samples were used for statistical analysis.

Statistical analysis

To determine the statistical difference between the test groups, a Student *t* test was performed in SigmaPlot 8 (Systat Software, San Jose, CA). The level of statistical significance was fixed at $P < 0.05$.

Results

Shockwave simulation

The propagation of LSW in the HM-3 lithotripter with the edge extender is simulated using the KZK equation (Fig. 1). It is clear that the tensile wave has been changed significantly after modifying the diffraction wave at the reflector aperture. At the focal point, the compressive waves are similar in amplitude and pulse duration (45.8 MPa *vs* 45.6 MPa and 0.96 μs *vs* 0.92 μs) as well as the peak negative pressure (-7.2 MPa *vs* −7.19 MPa in Fig. 1d). The tensile duration decreases significantly from 5.1 μs to 4 μs. The discrepancy between the arrival time of original and modified LSW increases from 0.16 μs at z = −70 mm to 0.48 μs at z = 70 mm. The diffraction wave, however, cannot be completely "blocked" by the acoustic absorbent materials with finite size because the production of the diffraction wave may also occur at the rim of the edge extender.

Pressure waveform and distribution

LSWs produced at the lithotripter focus at 20 kV were measured by LSHD, and representative waveforms are shown in Fig. 4. Using the edge extender, the compressive ◀F4

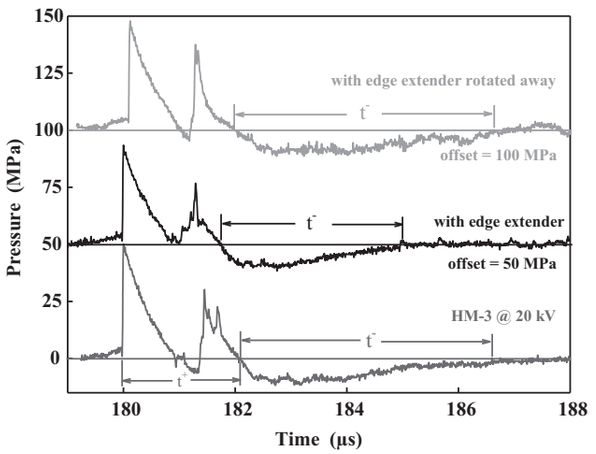

FIG. 4. Representative pressure waveforms measured by a light spot hydrophone at the focal point of the HM-3 lithotripter using the original reflector, the edge extender fitted with the aperture, and the edge extender rotated away at the output voltage of 20 kV.

Table 1. Peak Pressure and Temporal Parameters of the Shock Waves Produced by Different Reflector Configurations at Output Voltage of 20 KV

Lithotriper configuration	*p+ (MPa)*	*p− (MPa)*	*Beam width (mm)*	*t+ (μs)*	*t− (μs)*
Original HM-3	45.2 ± 3.8	−10.6 ± 0.7	8.7 × 12.7	1.98 ± 0.24	5.83 ± 0.56
With edge extender	44.6 ± 4.0	−11.1 ± 0.9	10.2 × 11.3	1.83 ± 0.1	3.2 ± 0.54

Beam width: −6 dB range of the peak positive pressure transverse to the lithotripter axis. t+: Positive pulse duration, measured by the zero- crossing duration of the first positive cycle of the shock wave. t-: Negative pulse duration, measured by the zero-crossing duration of the first negative cycle of the shock wave.

wave is almost unchanged, 44.6 ± 4.0 MPa in amplitude and 1.83 ± 0.11 μs in duration, in comparison with that of the original HM-3 reflector, 45.2 ± 3.8 MPa and 1.98 ± 0.24 μs without a statistical difference ($P = 0.15$ and 0.47, respectively), which confirms our hypothesis that modification of the diffraction wave at the lithotripter aperture has little effect on the center wave of LSW. The significance lies in the tensile part of the pressure waveform. Using the original HM-3 reflector, the tensile pressure is about −10.6 ± 0.7 MPa in amplitude and 5.83 ± 0.56 μs in duration. When the edge extender is fitted at the lithotripter aperture, however, the negative peak pressure is similar, −11.1 ± 0.9 MPa ($P = 0.24$), but the duration of the tensile wave decreases to 3.2 ± 0.54 μs ($P < 0.001$). Therefore, the acoustic energy for bubble cavitation becomes less. The changes on LSW profile are similar to the simulation results (Fig. 1).

The response of a 3-μm bubble nucleus to the measured waveforms at the lithotripter focus in Fig. 4 was then calculated using the Gilmore model.[20] For the original HM-3 reflector, the maximum bubble radius (R_{max}) is 986 μm and bubble collapse time (t_c) is 149 μs. In comparison, $R_{max} = 361$ μm is predicted for the lithotripter with the edge extender, corresponding to a 64% reduction in the maximum bubble expansion, and $t_c = 99$ μs. In addition, if all segments of the edge extender were rotated outward at the angle of ~120 degrees with respect to the lithotripter axis, the measured pressure waveform was similar to that of the original HM-3 reflector (Fig. 4) with predicted bubble response of $R_{max} = 897$ μm and $t_c = 135$ μs. Therefore, the tensile energy and the associated bubble cavitation can be restored.

T1 ▶ Table 1 summarizes the pressure amplitudes and temporal parameters of the LSWs at the focal zone of the Dornier HM-3 lithotripter. The pressure distribution of the peak positive (p^+) and peak negative (p^-) pressures of LSWs transverse to the lithotripter axis in the focal plane were also compared F5 ▶ (Fig. 5). It was found that pressure distribution patterns and −6 dB beam widths produced by the HM-3 lithotripter without and with the edge extender were similar (12.7 × 8.7 and 11.3 × 10.2 mm, respectively).

Acoustic emission

Using the passive cavitation detection method, AE signals associated with the dynamics of the bubble cluster generated by the LSWs were recorded.[14,32] Characteristic double burst structures were observed, and the bubble collapse time, defined as the time delay between these two AE bursts, is found to be proportional to R_{max}.[14] By using the edge extender, the bubble collapse time (175.8 ± 17.9 μs, mean ± standard deviation) is only 58% of that of the original HM-3 reflector at 20 kV F6 ▶ (324.4 ± 16.5 μs in Fig. 6a). The bubble collapse time in the HM-3 lithotripter increases from 230.7 ± 21.2 μs at 16 kV to 368.5 ± 24.3 μs at 24 kV. The corresponding values with use of the edge extender are 114.1 ± 14 μs at 16 kV and 209.4 ± 30.4 μs at 24 kV, respectively. Furthermore, the suppression effect on bubble cavitation is consistent throughout the focal zone of the lithotripter ($\Delta z = -20 \sim 6.5$ mm, $\Delta x = 0 \sim 13$ mm with reduction on the bubble collapse time ranging from 47.2% to 64.6% as shown in Fig. 6b and Fig. 6c, respectively).

Stone comminution

Using the phantom system (Fig. 3) designed to mimic stone comminution in the renal pelvis during SWL, the

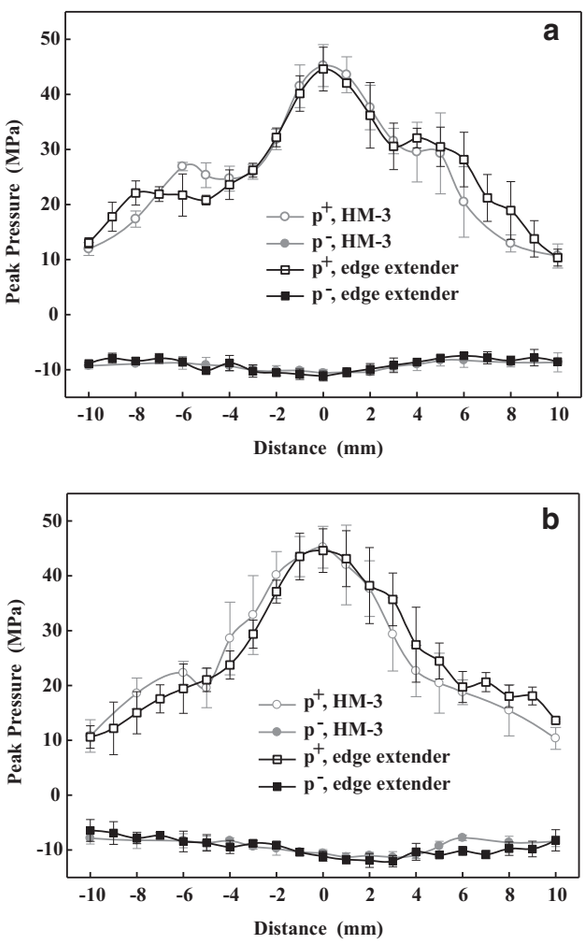

FIG. 5. Distributions of the peak pressure of the lithotripter shockwaves in the (a) foot-head and (b) left-right direction generated by using the original HM-3 reflector and the edge extender fitted with the aperture at 20 kV.

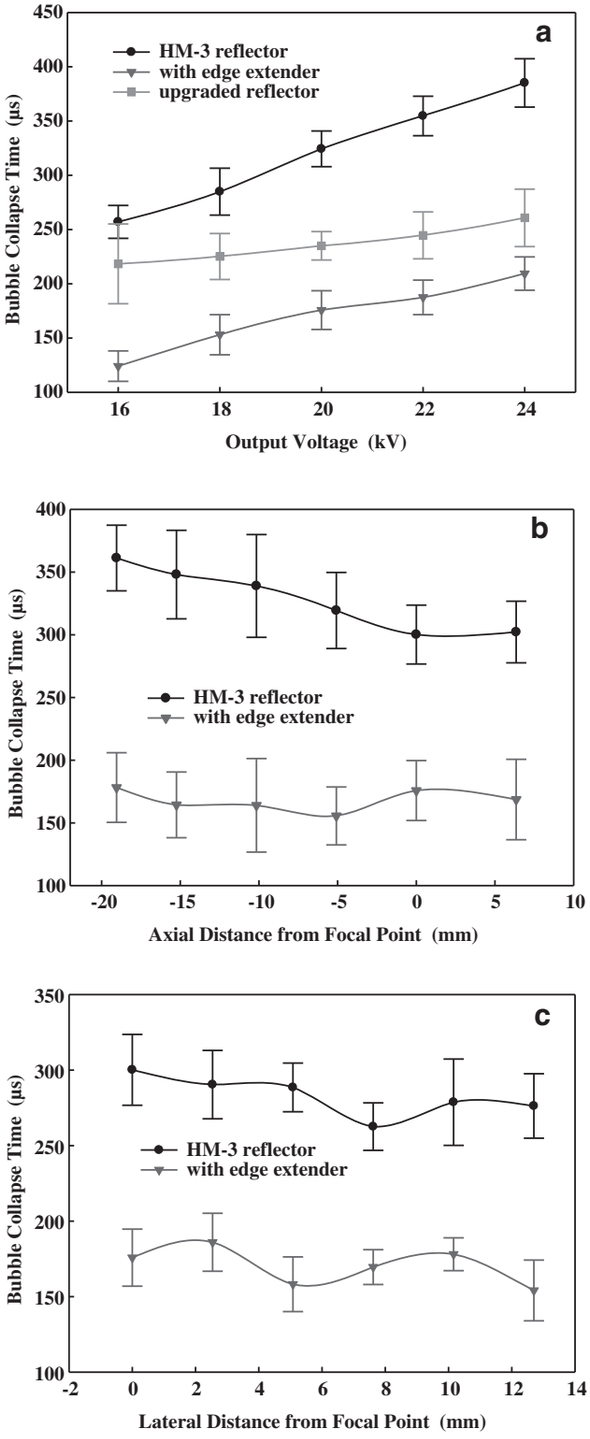

FIG. 6. Collapse time of the bubble cluster generated in water at the focal point of the Dornier HM-3 lithotripter with the original reflector, the upgraded reflector, and the edge extender (a) at the output voltage from 16 to 24 kV, (b) along the lithotripter axis and (c) transverse to the lithotripter axis in the focal plane.

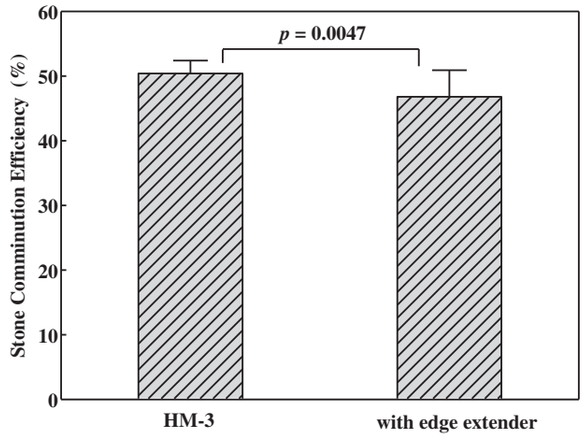

FIG. 7. The percentage of stone fragments made of plaster-of-Paris less than 2 mm after 200 shocks by using the original HM-3 reflector and the edge extender at 20 kV. A Student *t* test was performed to determine the statistical differences between the results.

fragmentation efficiencies produced by the HM-3 lithotripter were evaluated. As shown in Fig. 7, 46.8 ± 4.1% and ◀F7
50.4 ± 2.0% of stone mass were reduced to fragments less than 2 mm after 200 shocks produced by the HM-3 lithotripter at 20 kV with and without the edge extender, respectively, and there is no statistical difference ($P < 0.05$). Altogether, the stone comminution is satisfactory after modifying the diffraction wave at the lithotripter aperture in the early stage of SWL, which confirms our hypothesis that the edge extender has little effect on the center wave of LSW and, consequently, the initial disintegration of kidney calculus.

Rupture of vessel phantoms

The impact of the edge extender on vascular injury in SWL was investigated on a vessel phantom made of a regenerated cellulose hollow fiber. Using the original HM-3 reflector at 20 kV, the number of shocks needed to cause a rupture of the

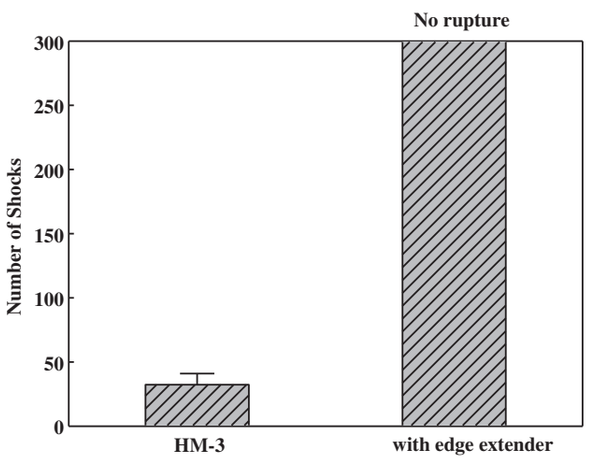

FIG. 8. Comparisons of the number of shocks to cause the rupture of the vessel phantom by using the original HM-3 reflector and the edge extender at 20 kV.

vessel phantom at the lithotripter focus is 32.3 ± 8.7. In comparison, using the edge extender fitted at the aperture, no rupture could be produced in the vessel phantom after 300 shocks (Fig. 8).

F8 ▶

Discussion

To suppress bubble cavitation at the focal zone of a lithotripter to enhance the safety of SWL treatment, a novel method has been devised by modifying the diffraction wave at the reflector aperture. This approach is derived from the theoretical simulation of acoustic wave propagation and evolution in the lithotripter field.[23] In this study, it is shown that such an approach can significantly reduce the bubble cavitation and, consequently, the potential for the vessel phantom rupture while producing satisfactory stone comminution. Afterward, the design, such as the segment's geometry, the angle with respect to the lithotripter axis, and the absorbent material, will be optimized in the following study. If the size of the edge extender is small enough to be accommodated in a water cushion, this method can be applied to most of the current dry-head lithotripters. This technical improvement, if confirmed *in vivo* and in clinics, could reduce the adverse effects and broaden the application scope of SWL, especially for those who are at much higher risk for SWL-induced chronic injury, such as elderly patients.[7,33]

Disintegration of renal calculi by SWL is a consequence of dynamic fracture of calculus caused by the growth and the coalescence of stress wave-induced microcracks (spalling, squeezing, and tear) inside the brittle stone,[1] and cavitation erosion on the exterior surface of calculus caused by the violent collapse of bubble cavitation (secondary shockwave or a liquid microject) [1,25,34] in a synergistic way.[28] Initially, stress waves dominate in breaking up kidney stones into distributed pieces. When the size of the residual fragments becomes less than half of the compressive wavelength in the stone, however, the effectiveness of stress waves will be hindered. In comparison, the erosion caused by the bubble cavitation weakens the stone structure, making it more fragile to the ensuing LSWs and associated bombardments of cavitation bubbles.

Altogether, stress wave-induced fracture is important in the initial disintegration of kidney stones, while cavitation is necessary to produce fine passable fragments. Therefore, the stone fragmentation may not be satisfactory if the bubble cavitation is suppressed throughout the SWL treatment, such as using the pressure release reflector.[13] To obtain a successful comminution of renal calculi, it is necessary to restore or enhance the bubble cavitation in the later stage—for example, after 500 shocks. *In vivo* SWL with a progressive increase of lithotripter output voltage or cavitation strength produced better stone fragmentation than protocols using constant or decreasing output voltage.[35] In addition, marked reduction of the glomerular filtration rate, renal plasma flow, and urinary sodium excretion in the kidney was observed after a number of shockwave deliveries.[36,37] This renal vasoconstriction effect is causally associated with a reduction in the number of cavitation bubble nuclei and the intraluminal volume of blood. These two factors will diminish the propensity for renal-parenchymal injury at subsequent higher pressure or cavitation exposure.[35] Therefore, gradually restoring bubble cavitation, which can be realized by rotating the edge extender outward, may lead to better stone fragmentation without increasing the propensity of vascular injury. This hypothesis will be investigated in the future *in vivo* study.

In comparison with the bubble collapse time using *in-situ* pulse superposition technique (Fig. 5a), modifying the edge wave seems more effective in suppressing bubble cavitation. It is interesting to notice that the relationships of the bubble collapse time with the output voltage with and without using the edge blocker are very similar. The *in-situ* pulse superposition methods, however, seem to become more dominant at higher output voltage, which is expected in the theoretical estimation because the larger amplitude of the second compressive wave coming from the uncovered bottom of the original HM-3 reflector provides more suppression effect on the bubble expansion induced by the leading LSW.[19] In addition, each segment of the edge extender is designed to work individually, which provides the feasibility of dynamically adjusting the suppression effect on bubble cavitation as the prototype reflector insert.[19] Characterization of the lithotripter field with different segment configurations (eg, the rotation angle) would allow us to further understand the mechanism of modifying the diffraction wave in the following investigation.

The focal zone of the lithotripter is ellipsoidal, 40 ~ 100 mm in length and 4 ~ 12 mm in width. Recent *in vitro* and numerical studies have shown that shear stress inside a stone induced by LSW is critical in the fragmentation.[38–40] When the focal width is greater than the stone size, fragmentation ability can be improved. With the progress of SWL, the fragments will spread out. Wide focus may ensure sufficient exposure of both stress wave and bubble cavitation to the residual pieces. Clinical reports have shown reduced stone-free rates and a great occurrence of adverse effects in patients who were treated with a narrow focal zone lithotripter.[41–44] Therefore, the beam width is a factor in the efficacy and safety of lithotripters.[45] By using the *in-situ* pulse superposition method, beam width was reduced from 14.3 × 9.6 mm to 5.9 × 6.6 mm.[23] In comparison, there is almost no change on the focal width using the edge extender.

Conclusion

Using the edge extender presented in this study, the contribution of the diffraction wave to the tensile component of LSW at the focal region could be reduced, leading to a significant and consistent suppression on bubble cavitation as confirmed by the measured bubble activities. Although some characteristics of LSWs are similar to those of the original HM-3 lithotripter (ie, compressive wave, the peak negative pressures, and focal width), the duration of the tensile wave was shortened significantly. Subsequently, the propensity of the vessel phantom injury was improved more than tenfold without compromising the stone fragmentation ability. Altogether, modifying the diffraction wave at the lithotripter aperture is effective in reducing bubble cavitation at the focal zone and may improve the safety of SWL.

Acknowledgments

The author thanks Dr. Jian Zhang for the valuable discussion and experiment assistance. This work was supported by National Institutes of Health grant R41 DK072910-01, USA.

AU1 ▶ **Disclosure Statement**

References

1. Chaussy C, Schmiedt E, Jocham D, et al. Extracorporeal shock wave lithotripsy. In: Chaussy C, ed. New Aspects in the Treatment of Kidney Stone Disease. Basel: Karger; 1982.
2. Lingeman JE. Extracorporeal shock wave lithotripsy. Development, instrumentation, and current status. Urol Clin North Am 1997;24:185–211.
3. Delius M. Medical applications and bioeffects of extracorporeal shock waves. Shock Waves 1994;4:55–72.
4. Evan AP, McAteer JA. Q-effects of shock wave lithotripsy. In: Coe FL, Favus MJ, Pak CY, Parks JH, Preminger GM, ed. Kidney Stones, Medical and Surgical Management. Philadephia: Lippincott-Raven Press, 1996, pp 549–570.
5. Willis LR, Evan AP, Connors BA, et al. Shockwave lithotripsy: Dose-related effects on renal structure, hemohynamics, and tubular function. J. Endourol 2005;19:90–101.
6. Skolarikos A, Alivizatos G, de la Rosette J. Extracorporeal shock wave lithotripsy 25 years later: Complications and their prevention. Eur Urol 2006;50:873–1128.
7. Evan AP, Willis LR, Lingeman JE, McAteer JA. Renal trauma and the risk of long-term complications in shock wave lithotripsy. Nephron 1998;78:1–8.
8. Sturtevant B. Shock wave physics of lithotriptors. In: Smith AD, Badlani GH, Bagley DH, et al, eds. Smith's Textbook of Endourology. St. Louis: Quality Medical, 1996, pp 529–552.
9. Freund JB, Colonius T, Evan AP. A cumulative shear mechanism for tissue damage initiation in shock-wave lithotripsy. Ultrasound Med Biol 2007;33:1495–1503.
10. Kodama T, Takayama K. Dynamic behavior of bubbles during extracorporeal shock-wave lithotripsy. Ultrasound Med Biol 1998;24:723–738.
11. Arndt R. Cavitation in fluid machinery and hydraulic structures. Ann Rev Fluid Mech 1981;13:273–328.
12. Takayama T, Nagoya H, Obara T, Kuwahara M. Application of holographic interferometric studies of underwater shock wave focusing to medicine. Proc SPIE Int Soc Optic Eng 1992:1029–1034.
13. Evan AP, Willis LR, McAteer JA, et al. Kidney damage and renal functional changes are minimized by waveform control that suppresses cavitation in shock wave lithotripsy. J Urol 2002;168:1556–1162.
14. Zhong P, Zhou YF, Zhu SL. Dynamics of bubble oscillation in constrained media and mechanisms of vessel rupture in SWL. Ultrasound Med Biol 2001;27:119–134.
15. Chen H, Brayman AA, Bailey MR, Matula TJ. Blood vessel rupture by cavitation. Urol Res 2010;38:321–326.
16. Bailey MR, Blackstock DT, Cleveland RO, Crum LA. Comparison of electrohydraulic lithotripters with rigid and pressure-release ellipsoidal reflectors. I. Acoustic fields. J Acoust Soc Am 1998;104:2517–2524.
17. Bailey MR, Blackstock DT, Cleveland RO, Crum LA. Comparison of electrohydraulic lithotripters with rigid and pressure-release ellipsoidal reflectors. II. Cavitation fields. J Acoust Soc Am 1999;106:1149–1160.
18. Delius M. Minimal static excess pressure minimises the effect of extracorporeal shock waves on cells and reduces it on gallstones. Ultrasound Med Biol 1997;23:611–617.
19. Zhong P, Zhou YF. Suppression of large intraluminal bubble expansion in shock wave lithotripsy without compromising stone comminution: Methodology and in vitro experiments. J Acoust Soc Am 2001;110:3283–3291.
20. Zhou Y, Zhong P. Suppression of large intraluminal bubble expansion in shock wave lithotripsy without compromising stone comminution: Refinement of reflector geometry. J Acoust Soc Am 2003;113:586–597.
21. Zhu S, Dreyer T, Liebler M, et al. Reduction of tissue injury in shock-wave lithotripsy by using an acoustic diode. Ultrasound Med Biol 2004;30:675–682.
22. Hamilton MF. Transient axial solution for the reflection of a spherical wave from a concave ellipsoidal mirror. J Acoust Soc Am 1993;106:102–112.
23. Zhou Y, Zhong P. The effect of reflector geometry on the acoustic field and bubble dynamics produced by an electrohydraulic shock wave lithotripter. J Acoust Soc Am 2006;119:3625–3636.
24. Averkiou MA, Cleveland RO. Modeling of an electrohydraulic lithotripter with the KZK equation. J Acoust Soc Am 1999;106:102–112.
25. Crum LA. Cavitation microjets as a contributory mechanism for renal calculi disintegration in ESWL. J Urol 1988;140: 1587–1590.
26. Rawlins AD. Diffraction of sound by a rigid screen with a soft or perfectly abosrbing edge. J Sound Vibrations 1976;45:53–67.
27. Bailey MR, Dalecki D, Child SZ, et al. Bioeffects of positive and negative acoustic pressures in vivo. J Acoust Soc Am 1996;100:3941–3946.
28. Zhu SL, Cocks FH, Preminger GM, Zhong P. The role of stress waves and cavitation in stone comminution in shock wave lithotripsy. Ultrasound Med Biol 2002;28:661–671.
29. Simmons WN, Zhou YF, Qin J, et al. Comparison of Light Spot Hydrophone (LSHD) and Fiber Optic Probe Hydrophone (FOPH) for lithotripter field characterization. Presented at the 2006 Annual Meeting of American Urological Association, May 20–25, 2006, Atlanta, GA.
30. Granz B, Nanke R, Fehr J, et al. Light spot hydrophone innovation in lithotripsy. Science Lithotripsy 2004:86–87.
31. Staudenraus J, Eisenmenger W. Fibre-optic probe hydrophone for ultrasonic and shock wave measurements. Ultrasonics 1993;31:267–273.
32. Cleveland RO, Sapozhnikov OA, Bailey MR, Crum LA. A dual passive cavitation detector for localized detection of lithotripsy-induced cavitation in vitro. J Acoust Soc Am 2000;107:1745–1758.
33. Lifshitz DA, Lingeman JE, Zafar FS, et al. Alterations in predicted growth rates of pediatric kidneys treated with extracorporeal shock wave lithotripsy. J Endourol 1998;12:469–475.
34. Blake JR, Gibson D. Cavitation bubbles near boundaries. 2. Free surface. J Fluid Mech 1987;181:197–212.
35. Maloney ME, Marguet CG, Zhou Y, et al. Progressive increase of lithotripter output produces better in-vivo stone comminution. J Endourol 2006;20:603–606.
36. Handa RK, Bailey MR, Paun M, et al. Pretreatment with low-energy shock waves induces renal vasoconstriction during standard shock wave lithotripsy (SWL): A treatment protocol known to reduce SWL-induced renal injury. BJU Int 2009;103:1270–1274.
37. Willis LR, Evan AP, Connors BA, et al. Shockwave lithotripsy: Dose-related effects on renal structure, hemodynamics, and tubular function. J Endourol 2005;19:90-101.
38. Cleveland RO, Sapozhnikov OA. Modeling elastic wave propagation in kidney stones with application to shock wave lithotripsy. J Acoust Soc Am 2005;118:2667-2676.
39. Sapozhnikov OA, Maxwell AD, MacConaghy B, Bailey MR. A mechanistic analysis of stone fracture in lithotripsy. J Acoust Soc Am 2007;121:1190–1202.

40. Qin J, Simmons WN, Sankin G, Zhong P. Effect of lithotripter focal width on stone comminution in shock wave lithotripsy. J Acoust Soc Am 2010;127:2635–2645.
41. Bierkens AF, Hendrikx AJ, de Kort VJ, et al. Efficacy of second generation lithotriptors: A multicenter comparative study of 2,206 extracorporeal shock wave lithotripsy treatments with the Siemens Lithostar, Dornier HM4, Wolf Piezolith 2300, Direx Tripter X-1 and Breakstone lithotriptors. J Urol 1992;148:1052–1057.
42. Evan AP, Willis LR: Extracorporeal shock wave lithotripsy: Complications. In: Smith AD, Badlani GH, Bagley DH, eds. Smith's Textbook of Endourology Ontario: BC Decker, 2007, pp 353–365.
43. Portis AJ, Yan Y, Pattaras JG, et al. Matched pair analysis of shock wave lithotripsy effectiveness for comparison of lithotriptors. J Urol 2003;169:58–62.
44. Tan EC, Tung KH, Foo KT. Comparative studies of extracorporeal shock wave lithotripsy by Dornier HM3, EDAP LT 01 and Sonolith 2000 devices. J Urol 1991;146:294–297.
45. Evan AP, McAteer JA, Connors BA, et al. Independent assessment of a wide-focus, low-pressure electromagnetic lithotripter: Absence of renal bioeffects in the pig. BJU Int 2008;101:382–388.

Address correspondence to:
Yufeng Zhou, Ph.D.
Division of Engineering Mechanics
School of Mechanical & Aerospace Engineering
Nanyang Technological University
Singapore 639798

E-mail: yfzhou@ntu.edu.sg

Abbreviations Used

AD = acoustic diode
AE = acoustic emission
KZK = Khokhlov-Zabolotskaya-Kuznetsov
LSHD = light spot hydrophone
LSW = lithotripsy shockwave
SWL = shockwave lithotripsy